Article

Monitoring Urban Deprived Areas with Remote Sensing and Machine Learning in Case of Disaster Recovery

Saman Ghaffarian [1,2,*] **and Sobhan Emtehani** [3]

1   Information Technology Group, Wageningen University & Research, 6700 EW Wageningen, The Netherlands
2   Business Economics Group, Wageningen University & Research, 6700 EW Wageningen, The Netherlands
3   Faculty of Geo-Information Science and Earth Observation (ITC), University of Twente,
    7500 AE Enschede, The Netherlands; s.emtehani@utwente.nl
*   Correspondence: saman.ghaffarian@wur.nl

Abstract: Rapid urbanization and increasing population in cities with a large portion of them settled in deprived neighborhoods, mostly defined as slum areas, have escalated inequality and vulnerability to natural disasters. As a result, monitoring such areas is essential to provide information and support decision-makers and urban planners, especially in case of disaster recovery. Here, we developed an approach to monitor the urban deprived areas over a four-year period after super Typhoon Haiyan, which struck Tacloban city, in the Philippines, in 2013, using high-resolution satellite images and machine learning methods. A Support Vector Machine classification method supported by a local binary patterns feature extraction model was initially performed to detect slum areas in the pre-disaster, just after/event, and post-disaster images. Afterward, a dense conditional random fields model was employed to produce the final slum areas maps. The developed method detected slum areas with accuracies over 83%. We produced the damage and recovery maps based on change analysis over the detected slum areas. The results revealed that most of the slum areas were reconstructed 4 years after Typhoon Haiyan, and thus, the city returned to the pre-existing vulnerability level.

Keywords: deprived areas; slums; disaster; recovery; damage; remote sensing; machine learning; SVM; SDG; Sendai Framework

1. Introduction

The United Nations (UN) estimates that 66% of the world population will live in urban areas by 2050, increasing from 54% in 2014 [1]. Most of this increase is expected to happen in developing countries located in Asia and Africa, which are currently facing different development challenges such as providing adequate accommodation for their increasing population [2]. Accordingly, the urbanization in the global south leads to a serious rise in urban poverty and thus expansion of deprived and informal urban areas (slums) [3,4]. This clearly depicts the need for better planning toward the corresponding Sustainable Development Goal (SDG) 11, i.e., Sustainable Cities and Communities. In addition, the rapid increase of population in cities and associated inequalities have escalated both the severity and impact of natural disasters in such areas, requiring effective disaster risk reduction strategies according to SDG 13, i.e., Climate Action.

Post-disaster recovery is one of the main components/phases of disaster risk management. Recovery is usually described as the process of reconstructing and returning communities to their pre-impact and normal conditions after a disaster [5,6], which can take years or decades. In the meantime, post-disaster recovery brings opportunity for the affected area, allowing them to identify and address their pre-existing vulnerabilities, including inequality, and better reconstruction of settlements, and improving the infrastructures and living conditions in deprived (slum) areas. This also addresses one of the action priorities of the Sendai Framework, which is to enhance disaster preparedness through the

build back better concept in the recovery and reconstruction process [7]. Consequently, providing information regarding the recovery process, including damage assessment after a disaster as well as reconstruction of deprived/slum areas, is critical to support decision-makers and recovery planners to effectively make decisions toward implementation of the build back better goal. Given that the urban deprived areas are one of the most vulnerable areas to disasters, decreasing of their size during the post-disaster recovery process is an indicator of successful build back better concept implementation.

Remote sensing (RS) data have become one of the main geospatial information sources to support the assessment of different components of disaster risk management [8] such as damage [9–11] and vulnerability [12,13] assessments. In addition, different data processing and machine learning methods were developed to extract information from RS data to support disaster risk management [10,14–16]. Only recently, a few studies addressed recovery assessment using RS, mostly focusing on the physical recovery assessment. For instance, Burton et al. [17] employed repeated photography to evaluate the post-Katrina reconstruction process in Mississippi. Brown et al. [18] used RS and survey data to assess the damage and early recovery after an earthquake. They showed that RS data could provide rapid support in terms of physical damage assessment. However, they extracted most of the information, e.g., building damages, manually. Hoshi et al. [19] used binary classification of RS data in addition to ground survey information to monitor post-disaster urban recovery. Contreras et al. [20] integrated high-resolution RS imagery and ground data to monitor the recovery process after the 2009 L'Aquila earthquake, in Italy. de Alwis Pitts and So [21] proposed a semi-automated object-based change detection method using pre-disaster map data and very high-resolution optical images to monitor buildings after the Kashmir earthquake, Pakistan. In addition, Derakhshan et al. [22] used remote sensing-based indices to monitor land cover changes in urban areas for post-earthquake recovery time. They showed the usefulness of such indices for general recovery assessment. All these studies demonstrated the importance of using RS in reducing the required ground data for post-disaster recovery assessment. Machine learning methods have been recently employed for post-disaster recovery monitoring. Sheykhmousa et al. [6] used Support Vector Machine (SVM) as the main classifier to assess the post-disaster recovery. They also conceptualized the recovery assessment using RS data and provided the information to translate the RS-derived land cover and land use changes to positive and negative recoveries. Random Forest classification executed in a cloud computing platform, i.e., Google Earth Engine [23] and Extreme Gradient Boosting (XGBoost) methods were also used to monitor the recovery [24]. Moreover, advanced deep learning methods, i.e., Convolutional Neural Network (CNN)-based approaches, were developed to extract information from very high-resolution satellite images [25] and update the building database [26]. These studies mostly focused on providing general information in recovery without investigating the build back better concept focusing on specific groups living in an urban area, i.e., slum dwellers.

There is no unique term or definition for deprived areas. "Informal settlement", "slum", and "inadequate housing" are examples of used terms [4]. In the current study, we consider the widely accepted term and definition provided by UN-Habitat that defines a slum household as a household or group of individuals with a lack of durable housing, adequate living space, safe water, sufficient sanitation, or security of tenure [27]. In addition, the physical appearance of the human settlements is one of the indicators of socio-economic status of dwellers, and thus, it can be employed to locate deprivation and discriminate it from other areas (e.g., formal settlements/buildings) in particular in urban areas [28,29]. Hence, remote sensing data due to providing spatial information and different physical features of the urban areas can be used for this purpose [30–32]. Remote sensing images have also been used to extract land cover and land use maps [33–36] as well as other urban objects [37–39]. Slum detection and extraction from remote sensing images was also the focus of several studies [40]. While early studies in this topic used traditional image processing methods [32,41–43], recent ones used more advanced machine learning

methods [44] such as SVM [45,46], Random Forest [47], and CNN-based approaches [48,49]. For example, Kuffer et al. [50] used gray-level co-occurrence matrix (GLCM) features to extract slum areas from very high-resolution images. They showed that such techniques could improve the accuracy of slum areas extraction. Ajami et al. [48] developed a deep learning-based method to identify the degree of deprivation from Very-High-Resolution (VHR) images. In addition, Wang et al. [30] developed a CNN-based method to identify the deprived pockets from VHR satellite images. However, their method requires extensive training samples to produce reliable accuracies. In another study, Wurm et al. [51] used a Random Forest classifier to map slum areas from Synthetic Aperture Radar (SAR) data. They showed that their developed machine learning method produces a high accuracy rate in extracting slum areas when combined with spatial features. However, the temporal changes of slum/deprived areas have not yet been studied in case of disaster recovery.

The aim of this study was to investigate the implementation of the build back better concept after a disaster, given that the presence of urban deprived areas is a proxy for vulnerability assessment [8], through the development of a robust machine learning approach to monitor temporal changes of deprived/slum areas in the recovery process. We developed a machine learning-based approach using SVM and Conditional Random Field (CRF) methods to extract slum areas from high-resolution satellite images for the pre, event, and post-disaster times. The slum areas were detected using the SVM method supported with Local Binary Patterns (LBP) features, and then, the DenseCRF [52] model was executed to refine the results and extract final slum areas for the selected time-lapse. In addition, the changes in slum areas were extracted to monitor their damage and recovery process. Tacloban city, located in the Leyte island, the Philippines, was selected to test the developed method. Accordingly, the damage and recovery of slums from super Typhoon Haiyan, which hit the area on 8 November 2013, were assessed, and implementation of the build back better concept was investigated in this area.

2. Materials and Methods

2.1. Case Study and Remote Sensing Data

Tacloban city is the largest city and the capital of Leyte province in the Philippines (Figure 1). Super Typhoon Haiyan (locally known as Yolanda) hit the area (the eye of the typhoon passed close to the south of Tacloban) causing massive damages. It was one of the strongest tropical typhoons ever landed worldwide [53]. It was also followed by a storm surge up to 5 m, which led to an increase in the number of fatalities mostly in the coastal neighborhoods [54].

Slum areas were detected from three high-resolution WorldView2 satellite images, which were acquired 8 months before (T0), 3 days after (T1), and 4 years after (T2) Haiyan, using our developed machine learning method (Table 1).

**Table 1.** Remote sensing images used in this study.

ID	Satellite	Acquisition Date	Spatial Resolution
T0		17 March 2013	
T1	WorldView2	11 November 2013	2 m
T2		18 March 2017	

2.2. Methods

Figure 2 illustrates the developed methodological framework to monitor slum areas and assess them in terms of the build back better concept. The developed approach consists of two main steps: (i) slum area extraction from high-resolution satellite images using the developed LBP-based SVM and fully/dense CRF (DenseCRF) methods, and (ii) generate damage and recovery maps and evaluate the build back better concept based on change detection.
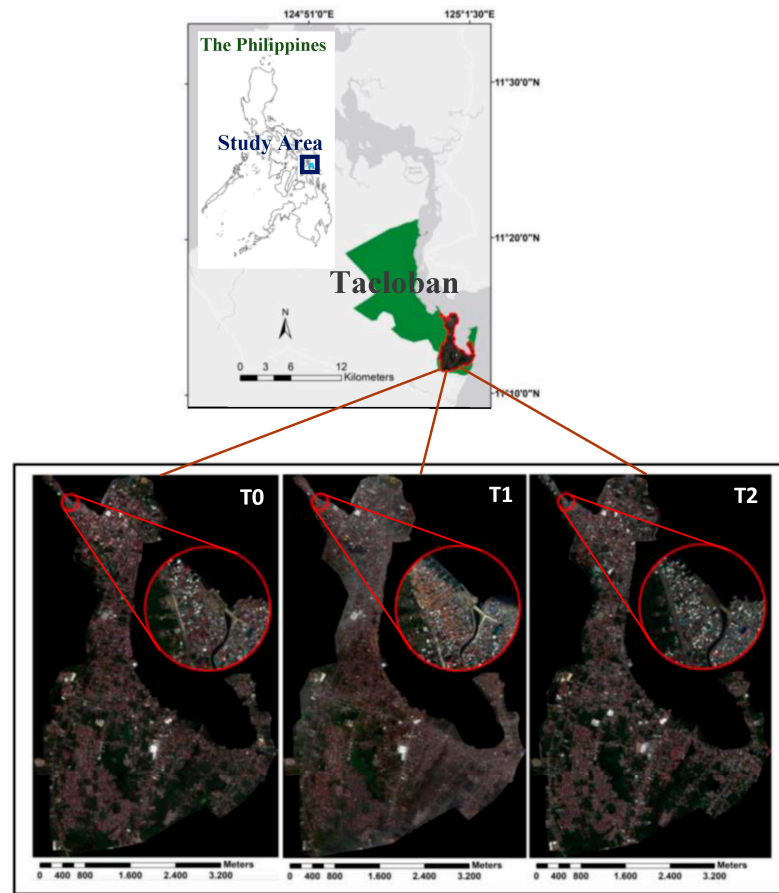
Figure 1. The overview of Tacloban, the Philippines, and the satellite images for the urban area acquired before (T0), 3 days after/event (T1), and 4 years after (T2) typhoon Haiyan. Red circles denote the slum areas in the northern part of Tacloban city, which were devastated by the typhoon.
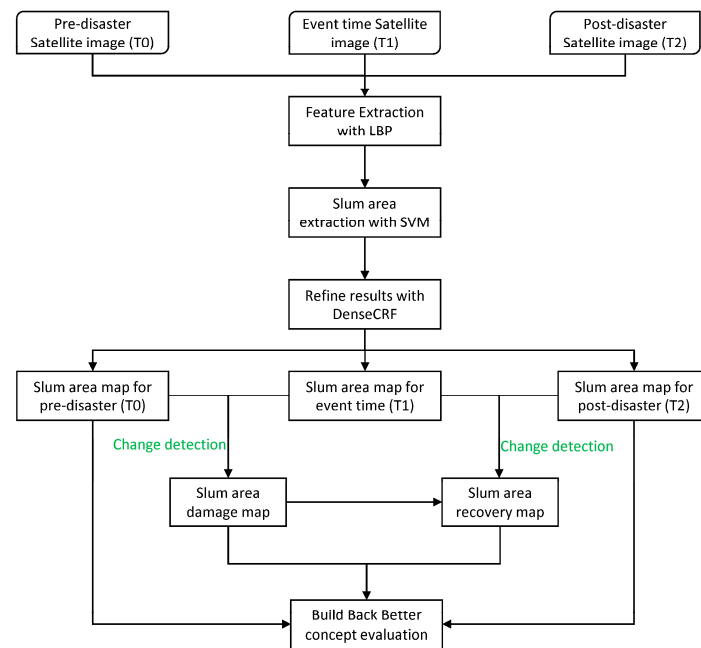
Figure 2. The proposed framework for slum area extraction and build back better concept evaluation from multi-temporal satellite images in case of disaster recovery.

2.2.1. Mapping Deprived Areas with SVM and DenseCRF

We used the Support Vector Machine (SVM) method as the main classifier to extract the deprived/slum areas from the high-resolution satellite images. SVM is a kernel-based non-parametric supervised machine learning algorithm, which is widely used for image classification tasks and produces reliable results [55–57]. SVM splits and groups the data by identifying a single linear boundary in its basic form. Thus, in such a case, the main goal of SVM is to determine an optimal line to separate the data into predefined classes using the training samples. SVM is popular due to its performance when only a small amount of training samples are available, contrary to deep learning methods that require big data for training [58–60]. SVM is well suited for urban area classification and object detection; in comparison to other machine learning algorithms, it produces competitive accuracy [6,61–63]. To execute the SVM classifier, we collected areas for both slum and non-slum areas from the images for each image separately. The selection of these areas was based on our field knowledge (field verification), and using different platforms including Google Earth Pro historical images, panchromatic very high-resolution satellite images and OpenStreetMap data to ensure the quality of the collected areas (Figure 3). Then, 70% of the areas were randomly selected to train the SVM method, and the rest were used for testing and accuracy assessment purposes.
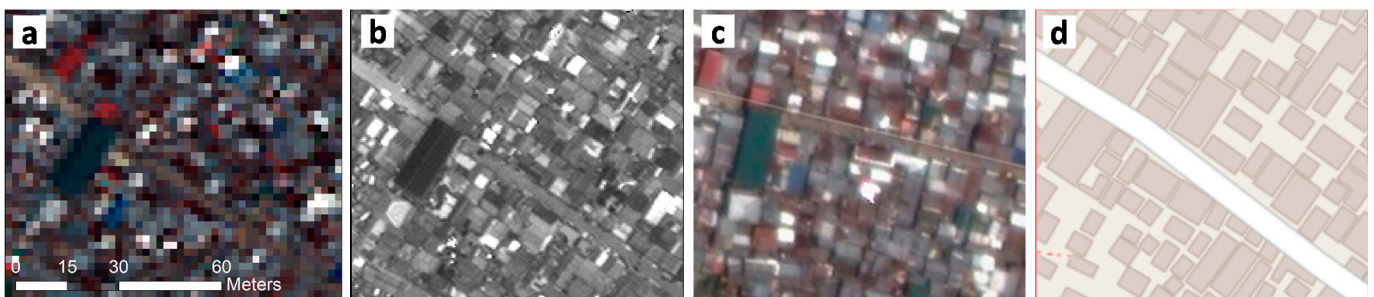
Figure 3. Examples of used data for training area selection. (**a**) Original satellite image used for slum detection, (**b**) panchromatic image, (**c**) Google Earth image, and (**d**) OpenStreetMap for before Haiyan time (i.e., 2013).

Due to the complexity of urban slum areas in terms of spectral and semantic definition, we used Local Binary Patterns (LBP) to support the SVM-based classification by providing feature layers. LBPs have been successfully used for different remote sensing image classification tasks. Researchers reported an increase in classification accuracies when used LBP features, in particular in areas with complex textural characteristics (e.g., slum areas) [24]. LBP is a powerful tool to discriminate and highlight textural features in the images using two parameters; lag distances (R) and windows sizes (P). We implemented LBP for each band of the satellite images with R = 4 and P = 8. Accordingly, we produced and added 8 textural layers to the original bands to be used for classification.

Yet after implementation of the SVM-LBP method, we verified inaccuracies mostly in the edge of the slum areas. Conditional Random Field (CRF) methods were used to refine and optimize the deep learning-based image classification results in edges, where abrupt changes happen in terms of textural characteristics and spectral values, and they demonstrated effective results [26]. Therefore, we used a fully/dense CRF model (DenseCRF) developed by [52] to alleviate the problem.

CRF iteratively evolves and computes labels and predictions to optimize the results using an energy function. The unary and pairwise potentials are the main components of the DenseCRF energy function. In this method, labels and their relations are considered as random variables and the edges in a graph-based theory, respectively, and they establish the conditional random fields.

Let l be the labels, extracted using SVM, for the input image. Then, the unary potential $\rho_x(l_x)$ is the probability of each pixel x, and the pairwise potential $\sigma_{x,y}(l_x, l_y)$ is the cost between labels at x, y pixels. Accordingly, the energy function can be computed as follows:

$$E(l) = \sum_x \rho_x(l_x) + \sum_{xy} \sigma_{xy}(l_x, l_y). \tag{1}$$

The pairwise potential consists of two Gaussian expressions. The first one uses both the location and color of the pixels in a kernel-based process of the similarity between adjacent pixels using the φ_α and φ_β parameters. The second one only uses the position of the pixels for smoothness based on the φ_γ parameter. Accordingly, the pairwise potential can be computed using the equation below:

$$\sigma_{x,y}(l_x, l_y) = \mu(l_x, l_y) \left[\omega_1 exp\left(-\frac{|p_x - p_y|^2}{2\varphi_\alpha^2} - \frac{|C_x - C_y|^2}{2\varphi_\alpha^2}\right) + \omega_2 exp\left(-\frac{|p_x - p_y|^2}{2\varphi_\alpha^2}\right) \right] \tag{2}$$

where p_x and C_x are the position and color vector for pixel x. $\mu(l_x, l_y)$ is defined based on the Potts model [64] and is equal to one if $l_x \neq l_y$; otherwise, it is equal to zero.

2.2.2. Accuracy Assessment

We evaluated the produced slum areas maps for each time step using overall, user's, and producer's accuracy measurements. Overall accuracy is computed by comparing all of the reference samples and their corresponding classified results to provide what proportion was classified correctly (usually expressed in percent). However, user's and producer's accuracies demonstrate the commission and omission errors, respectively. For accuracy assessment purpose, we selected a proportion of 30% of the collected areas at the start of the classification for slum and non-slum classes employing stratified random sampling and used them to calculate the accuracies [6,23,65].

2.2.3. Change Analysis

We generated the damage map by comparing the slum detection results for T0 and T1 times, and we provided the damaged and not-damaged classes. In addition, the recovery map was created by analyzing the changes in three time steps (T0–T2) and classifying them to four classes: (i) Not-damaged: refers to the areas that were slums in T0 and not damaged during the disaster; (ii) Recovered as slum: refers to the areas that were slums in T0 and have been recovered as slums in T2; (iii) Not-recovered or changed land use: refers to slum areas in T0 that were damaged during the disaster and have not been recovered as slum or changed their land use to other types (e.g., formal buildings) in T2; (iv) Newly built: refers to slum areas that were built after the disaster (in T2) while they were not slums before the disaster (T0). Moreover, we used the recovery and damage maps to evaluate the build back better concept, given that the slums are vulnerable areas to disasters and the reduction of such settlements contributes to the overall risk mitigation of the city, and thus, it can be considered as a positive sign of recovery and building back better.

3. Results and Discussion

Figure 4 shows the deprived/slum area detection results for the images acquired before (T0), 3 days after/event (T1), and 4 years after the disaster (T2). The detected slum areas are illustrated and overlaid on the original images by assigning a yellow color. Visual interpretation and qualitative analysis of the results show that the proposed method produced robust results in terms of detecting slum areas in such a challenging case study, which includes slums with different textural and spectral characteristics. The results also revealed that most of the slum areas are located close to the sea (i.e., coastal line), which is declared as the high-risk zone (also known as no-built area) after Typhoon Haiyan for such hazards. This also increases the vulnerability of those areas to typhoon and storm surge hazards due to their high exposure rate. In addition, there are big clusters of slums mostly

located in the northern part of the city, while also others are distributed in smaller clusters all over the city.
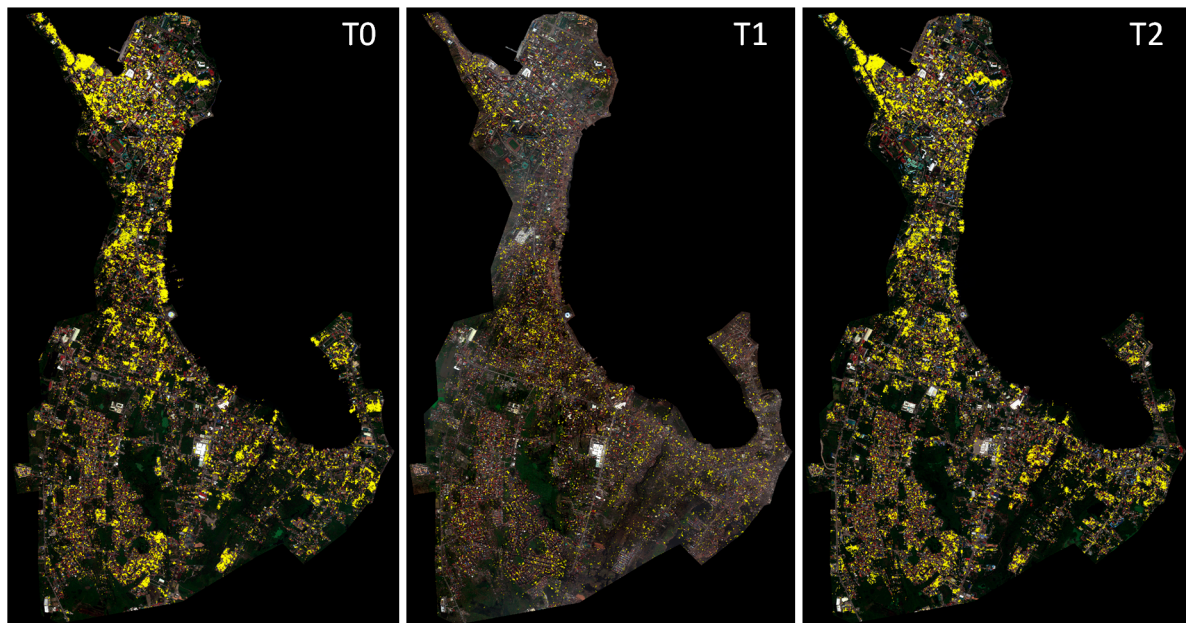
Figure 4. Detected slum areas, denoted in yellow color, for before (T0), 3 days after (T1), and 4 years after (T2) Haiyan.

The overall accuracies for the T0–T2 images were 84.2%, 83.2%, and 86.1% (Table 2). These results demonstrate the efficiency of the developed method in extracting slum areas for different time steps. In addition, producer's and user's accuracy were computed for each time step (Table 2). The worst user's and producer's accuracies were computed as 74.1% and 71.4%, respectively, for the event time image. Nevertheless, these are also fairly good results, since the presence of debris and rubbles and their similarity in terms of morphology, texture, and spectral characteristics mostly in the areas close to slums in an event time image makes the classification task even more challenging. However, the producer's accuracy values of the non-slum class in T0 and the slum class in T2 images demonstrate the relatively high omission errors. The presence of slums in between formal buildings and their vicinity, as well as the spectral proximity of the other image objects and features (e.g., roads), were other challenges faced in classifying the images and detecting slums.

Table 2. Accuracy assessment results for slum detection for 8 months before (T0), 3 days after (T1), and 4 years after (T2) after Typhoon Haiyan.

Time/ID	Pre-Disaster (T0)		Event Time (T1)		Post-Disaster (T2)	
Accuracy measure	Slum	Non-slum	Slum	Non-slum	Slum	Non-slum
Producer's accuracy (%)	93.3	76.8	71.4	90.1	76.2	93.2
User's accuracy (%)	76.4	93.5	74.1	88.9	88.9	84.6
Overall accuracy (%)	**84.2**		**83.2**		**86.1**	

Figure 5 shows the damage and recovery maps based on defined classes in Section 2.2.3 with different colors overlaid on the original post-disaster image. In the damage map, red and green colors illustrate the damaged and not-damaged areas, respectively. In addition, green, red, yellow, and blue colors illustrate not-damaged, not-recovered, or changed land use, recovered as slum, and newly built slum areas after Haiyan, respectively. Most of the slum areas were damaged during the disaster; almost all slums close to the coastal line are devastated and completely washed. In addition, most of the damaged slum areas are recovered/reconstructed as the same land use (slum area), which show no change in the vulnerability rate of the area, and thus, the build back better goal has not been reached

in Tacloban city after 4 years. For example, the area in the northern part of Tacloban city, denoted as "a" (Figure 5), is recovered as slum area just next to the sea, which was announced as a high-risk/danger zone. However, rarely positive recoveries can be seen in the recovery map, where the previous slum areas are changed to other land use types (e.g., formal buildings) or completely removed/relocated from the danger zone (e.g., the area denoted as "b" in Figure 5).
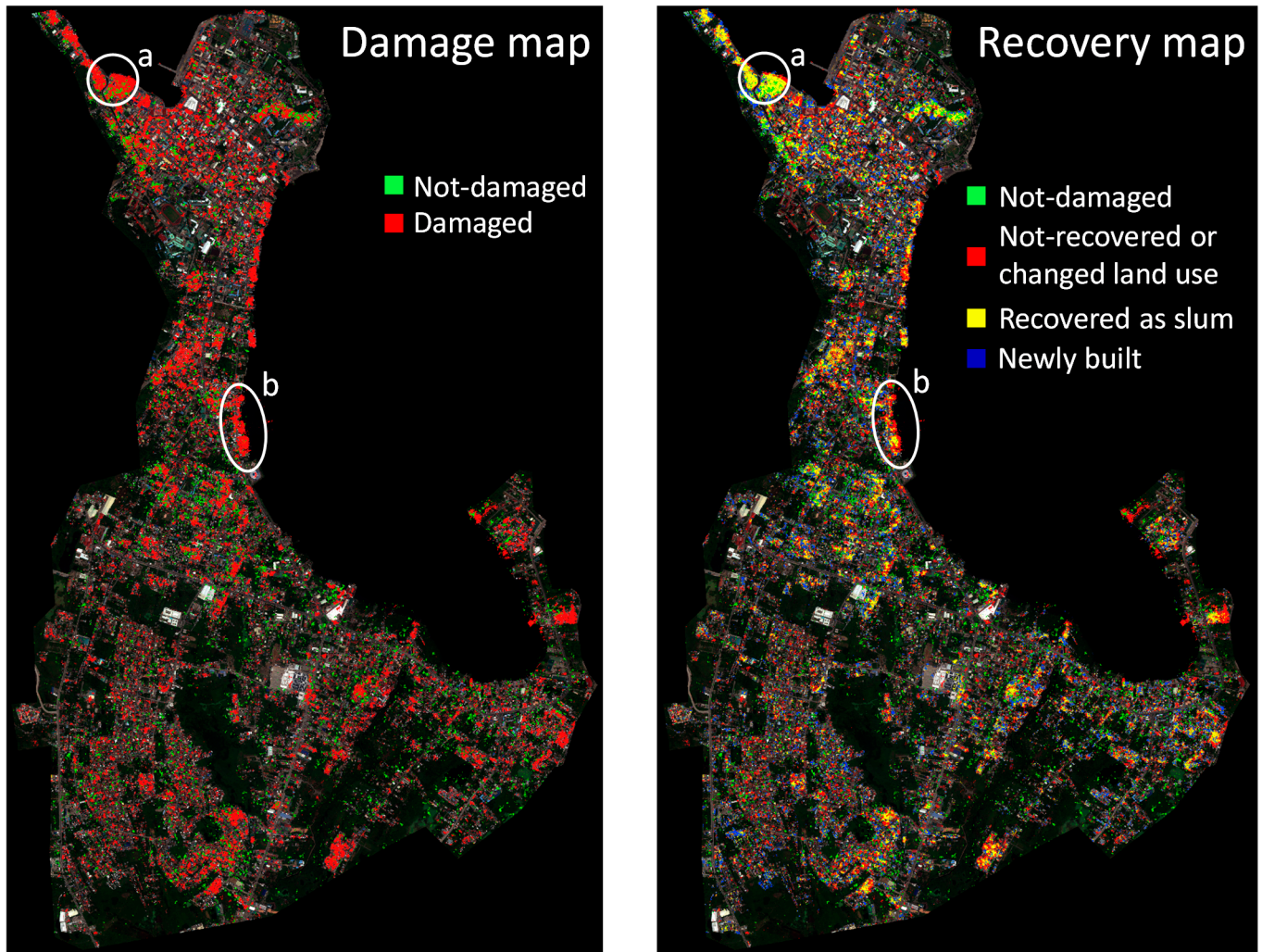
Figure 5. Damage and recovery maps for slum areas after Typhoon Haiyan, and the denoted areas as "a" and "b" show the negative and positive build-back-better goal implementation, respectively.

4. Conclusions

The aim of this study was to monitor the urban deprived areas after Typhoon Haiyan, which hit Tacloban city in the Philippines in November 2013. In addition, we analyze and discuss the results from the build back better perspective defined in the Sendai Framework. For this, we developed a machine learning-based approach based on SVM and DenseCRF models to classify the high-resolution satellite images acquired 8 months before, 3 days after the event, and 4 years after the disaster and detected slum areas, which are accepted as the deprived urban areas. The measured accuracy values for the classification results show the robustness of the proposed method in extracting slum areas in such challenging environment even in an event time image, which contains debris and rubble land covers. Then, we generated the corresponding damage and recovery maps, showing the damaged, recovered, not-recovered, and newly built slums and discussed them from the vulnerability

assessment and the build back better point of view. The developed methods can be used to monitor and evaluate the urban deprived areas in any other location or in case of any type of disaster. For this, the parameters of the machine learning methods should be fine-tuned for the specific case study and extract slum areas from multi-temporal remote sensing images. However, using additional data types such as survey data can contribute to a more comprehensive social vulnerability assessment [24], and thus, better evaluations in terms of the build back better concept. Moreover, using deep learning, in particular, CNN-based methods can increase the accuracy of the detection work where we have a large amount of data available to train such models.

Author Contributions: Conceptualization, S.G. and S.E.; methodology, S.G. and S.E.; validation, S.G.; formal analysis, S.G. and S.E.; data curation, S.G. and S.E.; writing—review and editing, S.G. and S.E. All authors have read and agreed to the published version of the manuscript.

Conflicts of Interest: The authors declare no conflict of interest.

References

1. United Nations. *World Urbanization Prospects, the 2014 Revision*; United Nations: New York, NY, USA, 2014.
2. Mahabir, R.; Crooks, A.; Croitoru, A.; Agouris, P. The study of slums as social and physical constructs: Challenges and emerging research opportunities. *Reg. Stud. Reg. Sci.* **2016**, *3*, 399–419. [CrossRef]
3. Mahabir, R.; Croitoru, A.; Crooks, A.T.; Agouris, P.; Stefanidis, A. A critical review of high and very high-resolution remote sensing approaches for detecting and mapping slums: Trends, challenges and emerging opportunities. *Urban Sci.* **2018**, *2*, 8. [CrossRef]
4. Thomson, D.R.; Kuffer, M.; Boo, G.; Hati, B.; Grippa, T.; Elsey, H.; Linard, C.; Mahabir, R.; Kyobutungi, C.; Maviti, J.; et al. Need for an integrated deprived area "slum" mapping system (ideamaps) in low- and middle-income countries (lmics). *Soc. Sci.* **2020**, *9*, 80. [CrossRef]
5. Chang, S.E. Urban disaster recovery: A measurement framework and its application to the 1995 kobe earthquake. *Disasters* **2010**, *34*, 303–327. [CrossRef]
6. Sheykhmousa, M.; Kerle, N.; Kuffer, M.; Ghaffarian, S. Post-disaster recovery assessment with machine learning-derived land cover and land use information. *Remote Sens.* **2019**, *11*, 1174. [CrossRef]
7. UNISDR. Sendai framework for disaster risk reduction 2015–2030. In Proceedings of the Third World Conference Disaster Risk Reduction, Sendai, Japan, 14–18 March 2015; pp. 1–25.
8. Ghaffarian, S.; Kerle, N.; Filatova, T. Remote sensing-based proxies for urban disaster risk management and resilience: A review. *Remote Sens.* **2018**, *10*, 1760. [CrossRef]
9. Kerle, N.; Nex, F.; Gerke, M.; Duarte, D.; Vetrivel, A. Uav-based structural damage mapping: A review. *ISPRS Int. J. Geo-Inf.* **2019**, *9*, 14. [CrossRef]
10. Nex, F.; Duarte, D.; Tonolo, F.G.; Kerle, N. Structural building damage detection with deep learning: Assessment of a state-of-the-art cnn in operational conditions. *Remote Sens.* **2019**, *11*, 2765. [CrossRef]
11. Ghaffarian, S.; Kerle, N. Towards post-disaster debris identification for precise damage and recovery assessments from uav and satellite images. *Int. Arch. Photogramm. Remote Sens. Spat. Inf. Sci.* **2019**, *XLII-2/W13*, 297–302. [CrossRef]
12. Ebert, A.; Kerle, N.; Stein, A. Urban social vulnerability assessment with physical proxies and spatial metrics derived from air- and spaceborne imagery and gis data. *Nat. Hazards* **2009**, *48*, 275–294. [CrossRef]
13. Harb, M.M.; De Vecchi, D.; Dell'Acqua, F. Phisical vulnerability proxies from remotes sensing: Reviewing, implementing and disseminating selected techniques. *IEEE Geosci. Remote Sens. Mag.* **2015**, *3*, 20–33. [CrossRef]
14. Lary, D.J.; Alavi, A.H.; Gandomi, A.H.; Walker, A.L. Machine learning in geosciences and remote sensing. *Geosci. Front.* **2016**, *7*, 3–10. [CrossRef]
15. Ma, L.; Liu, Y.; Zhang, X.; Ye, Y.; Yin, G.; Johnson, B.A. Deep learning in remote sensing applications: A meta-analysis and review. *ISPRS J. Photogramm. Remote Sens.* **2019**, *152*, 166–177. [CrossRef]
16. Tilon, S.; Nex, F.; Kerle, N.; Vosselman, G. Post-disaster building damage detection from earth observation imagery using unsupervised and transferable anomaly detecting generative adversarial networks. *Remote Sens.* **2020**, *12*, 4193. [CrossRef]
17. Burton, C.; Mitchell, J.T.; Cutter, S.L. Evaluating post-katrina recovery in mississippi using repeat photography. *Disasters* **2011**, *35*, 488–509. [CrossRef] [PubMed]

18. Brown, D.; Saito, K.; Liu, M.; Spence, R.; So, E.; Ramage, M. The use of remotely sensed data and ground survey tools to assess damage and monitor early recovery following the 12.5.2008 wenchuan earthquake in china. *Bull. Earthq. Eng.* **2011**, *10*, 741–764. [CrossRef]

19. Hoshi, T.; Murao, O.; Yoshino, K.; Yamazaki, F.; Estrada, M. Post-disaster urban recovery monitoring in pisco after the 2007 peru earthquake using satellite image. *J. Disaster Res.* **2014**, *9*, 1059–1068. [CrossRef]

20. Contreras, D.; Blaschke, T.; Tiede, D.; Jilge, M. Monitoring recovery after earthquakes through the integration of remote sensing, gis, and ground observations: The case of l'aquila (italy). *Cartogr. Geogr. Inf. Sci.* **2016**, *43*, 115–133. [CrossRef]

21. de Alwis Pitts, D.A.; So, E. Enhanced change detection index for disaster response, recovery assessment and monitoring of buildings and critical facilities—a case study for muzzaffarabad, pakistan. *Int. J. Appl. Earth Obs. Geoinf.* **2017**, *63*, 167–177. [CrossRef]

22. Derakhshan, S.; Cutter, S.L.; Wang, C. Remote sensing derived indices for tracking urban land surface change in case of earthquake recovery. *Remote Sens.* **2020**, *12*, 895. [CrossRef]

23. Ghaffarian, S.; Rezaie Farhadabad, A.; Kerle, N. Post-disaster recovery monitoring with google earth engine. *Appl. Sci.* **2020**, *10*, 4574. [CrossRef]

24. Kerle, N.; Ghaffarian, S.; Nawrotzki, R.; Leppert, G.; Lech, M. Evaluating resilience-centered development interventions with remote sensing. *Remote Sens.* **2019**, *11*, 2511. [CrossRef]

25. Ghaffarian, S.; Kerle, N. Post-disaster recovery assessment using multi-temporal satellite images with a deep learning approach. In Proceedings of the 39th EARSeL Conference, Salzburg, Austria, 1–4 July 2019.

26. Ghaffarian, S.; Kerle, N.; Pasolli, E.; Jokar Arsanjani, J. Post-disaster building database updating using automated deep learning: An integration of pre-disaster openstreetmap and multi-temporal satellite data. *Remote Sens.* **2019**, *11*, 2427. [CrossRef]

27. UN-Habitat. Slums: Some Definitions; Nairobi: Un-habitat. Available online: https://mirror.unhabitat.org/documents/media_centre/sowcr2006/SOWCR%205.pdf (accessed on 27 March 2021).

28. Taubenböck, H.; Wegmann, M.; Roth, A.; Mehl, H.; Dech, S. Urbanization in india—Spatiotemporal analysis using remote sensing data. *Comput. Environ. Urban Syst.* **2009**, *33*, 179–188. [CrossRef]

29. Arribas-Bel, D.; Patino, J.E.; Duque, J.C. Remote sensing-based measurement of living environment deprivation: Improving classical approaches with machine learning. *PLoS ONE* **2017**, *12*, e0176684. [CrossRef] [PubMed]

30. Wang, J.; Kuffer, M.; Roy, D.; Pfeffer, K. Deprivation pockets through the lens of convolutional neural networks. *Remote Sens. Environ.* **2019**, *234*, 111448. [CrossRef]

31. Graesser, J.; Cheriyadat, A.; Vatsavai, R.R.; Chandola, V.; Long, J.; Bright, E. Image based characterization of formal and informal neighborhoods in an urban landscape. *IEEE J. Sel. Top. Appl. Earth Obs. Remote Sens.* **2012**, *5*, 1164–1176. [CrossRef]

32. Kohli, D.; Sliuzas, R.; Kerle, N.; Stein, A. An ontology of slums for image-based classification. *Comput. Environ. Urban Syst.* **2012**, *36*, 154–163. [CrossRef]

33. Tong, X.-Y.; Xia, G.-S.; Lu, Q.; Shen, H.; Li, S.; You, S.; Zhang, L. Land-cover classification with high-resolution remote sensing images using transferable deep models. *Remote Sens. Environ.* **2020**, *237*, 111322. [CrossRef]

34. Abdi, A.M. Land cover and land use classification performance of machine learning algorithms in a boreal landscape using sentinel-2 data. *Gisci. Remote Sens.* **2020**, *57*, 1–20. [CrossRef]

35. Zhang, C.; Sargent, I.; Pan, X.; Li, H.; Gardiner, A.; Hare, J.; Atkinson, P.M. Joint deep learning for land cover and land use classification. *Remote Sens. Environ.* **2019**, *221*, 173–187. [CrossRef]

36. Ghaffarian, S.; Ghaffarian, S. Automatic histogram-based fuzzy c-means clustering for remote sensing imagery. *ISPRS J. Photogramm. Remote Sens.* **2014**, *97*, 46–57. [CrossRef]

37. Ghaffarian, S.; Ghaffarian, S. Automatic building detection based on purposive fastica (pfica) algorithm using monocular high resolution google earth images. *ISPRS J. Photogramm. Remote Sens.* **2014**, *97*, 152–159. [CrossRef]

38. Jiao, L.; Zhang, F.; Liu, F.; Yang, S.; Li, L.; Feng, Z.; Qu, R. A survey of deep learning-based object detection. *IEEE Access* **2019**, *7*, 128837–128868. [CrossRef]

39. Ghaffarian, S.; Gokasar, I. Automatic vehicle detection based on automatic histogram-based fuzzy c- means algorithm and perceptual grouping using very high-resolution aerial imagery and road vector data. *J. Appl. Remote Sens.* **2016**, *10*, 015011. [CrossRef]

40. Kuffer, M.; Pfeffer, K.; Sliuzas, R. Slums from space—15 years of slum mapping using remote sensing. *Remote Sens.* **2016**, *8*, 455. [CrossRef]

41. Kuffer, M.; Barrosb, J. Urban morphology of unplanned settlements: The use of spatial metrics in vhr remotely sensed images. *Procedia Environ. Sci.* **2011**, *7*, 152–157. [CrossRef]

42. Kohli, D.; Sliuzas, R.; Stein, A. Urban slum detection using texture and spatial metrics derived from satellite imagery. *J. Spat. Sci.* **2016**, *61*, 405–426. [CrossRef]

43. Fallatah, A.; Jones, S.; Mitchell, D.; Kohli, D. Mapping informal settlement indicators using object-oriented analysis in the middle east. *Int. J. Digit. Earth* **2019**, *12*, 802–824. [CrossRef]

44. Gadiraju, K.K.; Vatsavai, R.R.; Kaza, N.; Wibbels, E.; Krishna, A. Machine learning approaches for slum detection using very high resolution satellite images. In Proceedings of the 2018 IEEE International Conference on Data Mining Workshops (ICDMW), Singapore, 17–20 November 2018; pp. 1397–1404.

45. Duque, J.C.; Patino, J.E.; Betancourt, A. Exploring the potential of machine learning for automatic slum identification from vhr imagery. *Remote Sens.* **2017**, *9*, 895. [CrossRef]

46. Ranguelova, E.; Weel, B.; Roy, D.; Kuffer, M.; Pfeffer, K.; Lees, M. Image based classification of slums, built-up and non-built-up areas in kalyan and bangalore, india. *Eur. J. Remote Sens.* **2019**, *52*, 40–61. [CrossRef]

47. Leonita, G.; Kuffer, M.; Sliuzas, R.; Persello, C. Machine learning-based slum mapping in support of slum upgrading programs: The case of bandung city, indonesia. *Remote Sens.* **2018**, *10*, 1522. [CrossRef]

48. Ajami, A.; Kuffer, M.; Persello, C.; Pfeffer, K. Identifying a slums' degree of deprivation from vhr images using convolutional neural networks. *Remote Sens.* **2019**, *11*, 1282. [CrossRef]

49. Verma, D.; Jana, A.; Ramamritham, K. Transfer learning approach to map urban slums using high and medium resolution satellite imagery. *Habitat Int.* **2019**, *88*, 101981. [CrossRef]

50. Kuffer, M.; Pfeffer, K.; Sliuzas, R.; Baud, I. Extraction of slum areas from vhr imagery using glcm variance. *IEEE J. Sel. Top. Appl. Earth Obs. Remote Sens.* **2016**, *9*, 1830–1840. [CrossRef]

51. Wurm, M.; Taubenböck, H.; Weigand, M.; Schmitt, A. Slum mapping in polarimetric sar data using spatial features. *Remote Sens. Environ.* **2017**, *194*, 190–204. [CrossRef]

52. Krähenbühl, P.; Koltun, V. Efficient inference in fully connected crfs with gaussian edge potentials. *Adv. Neural Inf. Process Syst.* **2011**, *4*, 109–117.

53. Mori, N.; Kato, M.; Kim, S.; Mase, H.; Shibutani, Y.; Takemi, T.; Tsuboki, K.; Yasuda, T. Local amplification of storm surge by super typhoon haiyan in leyte gulf. *Geophys. Res. Lett.* **2014**, *41*, 5106–5113. [CrossRef] [PubMed]

54. Ching, P.K.; de Los Reyes, V.C.; Sucaldito, M.N.; Tayag, E. An assessment of disaster-related mortality post-haiyan in tacloban city. *West. Pac. Surveill. Response J.* **2015**, *6*, 34. [CrossRef] [PubMed]

55. Mountrakis, G.; Im, J.; Ogole, C. Support vector machines in remote sensing: A review. *ISPRS J. Photogramm. Remote Sens.* **2011**, *66*, 247–259. [CrossRef]

56. Sheykhmousa, M.; Mahdianpari, M.; Ghanbari, H.; Mohammadimanesh, F.; Ghamisi, P.; Homayouni, S. Support vector machine versus random forest for remote sensing image classification: A meta-analysis and systematic review. *IEEE J. Sel. Top. Appl. Earth Obs. Remote Sens.* **2020**, *13*, 6308–6325. [CrossRef]

57. Eggen, M.; Ozdogan, M.; Zaitchik, B.F.; Simane, B. Land cover classification in complex and fragmented agricultural landscapes of the ethiopian highlands. *Remote Sens.* **2016**, *8*, 1020. [CrossRef]

58. Vetrivel, A.; Gerke, M.; Kerle, N.; Vosselman, G. Identification of structurally damaged areas in airborne oblique images using a visual-bag-of-words approach. *Remote Sens.* **2016**, *8*, 231. [CrossRef]

59. Zafari, A.; Zurita-Milla, R.; Izquierdo-Verdiguier, E. Evaluating the performance of a random forest kernel for land cover classification. *Remote Sens.* **2019**, *11*, 575. [CrossRef]

60. Hussain, M.; Chen, D.; Cheng, A.; Wei, H.; Stanley, D. Change detection from remotely sensed images: From pixel-based to object-based approaches. *ISPRS J. Photogramm. Remote Sens.* **2013**, *80*, 91–106. [CrossRef]

61. Mboga, N.; Persello, C.; Bergado, J.; Stein, A. Detection of informal settlements from vhr images using convolutional neural networks. *Remote Sens.* **2017**, *9*, 1106. [CrossRef]

62. Turker, M.; Koc-San, D. Building extraction from high-resolution optical spaceborne images using the integration of support vector machine (svm) classification, hough transformation and perceptual grouping. *Int. J. Appl. Earth Obs. Geoinf.* **2015**, *34*, 58–69. [CrossRef]

63. Koc San, D.; Turker, M. Support vector machines classification for finding building patches from ikonos imagery: The effect of additional bands. *J. Appl. Remote Sens.* **2014**, *8*, 083694. [CrossRef]

64. Potts, R.B. Some generalized order-disorder transformations. In *Mathematical Proceedings of the Cambridge Philosophical Society*; Cambridge University Press: Cambridge, UK, 1952; Volume 48, pp. 106–109.

65. Marsett, R.C.; Qi, J.; Heilman, P.; Biedenbender, S.H.; Carolyn Watson, M.; Amer, S.; Weltz, M.; Goodrich, D.; Marsett, R. Remote sensing for grassland management in the arid southwest. *Rangel. Ecol. Manag.* **2006**, *59*, 530–540. [CrossRef]